Biochimica et Biophysica Acta 1807 (2011) 368–374

Contents lists available at ScienceDirect

Biochimica et Biophysica Acta

journal homepage: www.elsevier.com/locate/bbabio

# Fine structure of granal thylakoid membrane organization using cryo electron tomography

Roman Kouřil *, Gert T. Oostergetel, Egbert J. Boekema *

*Electron microscopy group, Groningen Biomolecular Sciences and Biotechnology Institute, University of Groningen, Groningen, The Netherlands*

ARTICLE INFO

*Article history:*
Received 19 October 2010
Received in revised form 15 November 2010
Accepted 17 November 2010
Available online 24 November 2010

*Keywords:*
Thylakoid membrane
Photosystem II
Supercomplex
Electron microscopy
Cryo tomography

ABSTRACT

The architecture of grana membranes from spinach chloroplasts was studied by cryo electron tomography. Tomographic reconstructions of ice-embedded isolated grana stacks enabled to resolve features of photosystem II (PSII) in the native membrane and to assign the absolute orientation of individual membranes of granal thylakoid discs. Averaging of 3D sub-volumes containing PSII complexes provided a 3D structure of the PSII complex at 40 Å resolution. Comparison with a recently proposed pseudo-atomic model of the PSII supercomplex revealed the presence of unknown protein densities right on top of 4 light harvesting complex II (LHCII) trimers at the lumenal side of the membrane. The positions of individual dimeric PSII cores within an entire membrane layer indicates that about 23% supercomplexes must be of smaller size than full $C_2S_2M_2$ supercomplexes, to avoid overlap.



## 1. Introduction

Chloroplasts play a central role in the plant energy metabolism known as photosynthesis. They enclose the thylakoid membrane, which forms a unique three-dimensional network with regular stacks of thylakoids, called grana, which are interconnected by single membranes, the stroma thylakoids. The distinct parts of the thylakoid membrane specifically accommodate individual components of photosynthetic apparatus. Photosystem II (PSII) and the light-harvesting complex II (LHCII) are confined mainly to grana stacks, whereas most of Photosystem I (PSI), the light-harvesting complex I and ATP synthase are localized in unstacked stromal thylakoids and grana margins. Distribution of cytochrome $b_6f$ complex in the thylakoid membrane seems to be unrestricted [1].

PSII consists of a dimeric core complex and a peripheral antenna system composed of 6 different complexes, belonging to the Lhcb (Light-harvesting complex) multigenic family [2]. The major antenna complex, LHCII, is organized in heterotrimers composed of the products of the *Lhcb1-3* genes. The three other subunits, CP29 (Lhcb4), CP26 (Lhcb5) and CP24 (Lhcb6) are present as monomers. A variable number of the peripheral antenna proteins can associate with dimeric PSII core complexes to form the so-called PSII-LHCII supercomplexes [3]. Many supercomplexes observed in spinach and *Arabidopsis thaliana* contain a dimeric core ($C_2$), 2 LHCII trimers (trimer S) strongly bound to the complex on the side of CP43 and CP26, and 2 more trimers, moderately bound (trimer M), which are in contact with CP29 and CP24. This complex is known as the $C_2S_2M_2$ supercomplex [3]. Occasionally, spinach supercomplexes loosely bind a third trimer (trimer L) around CP24 [4]. A 3D reconstruction of a smaller supercomplex containing only one trimer per reaction center and lacking CP24 ($C_2S_2$) was obtained by cryo-EM at about 17 Å resolution [5,6]. More recently, a 2D map at 12 Å resolution was obtained and used to generate a pseudo-atomic 3D model. This allowed determination of the location and orientation of individual light-harvesting components and the approximate position of pigments [7].

The lateral distribution of protein complexes within grana membranes is an intriguing topic and was a subject of many structural studies using electron microscopy of either freeze-fractured or negatively stained grana membranes (see [3,8] for reviews), atomic force microscopy [9] or, very recently, by cryo electron tomography [10]. Although in most grana membranes PSII supercomplexes are not highly organized, semi-crystalline domains of PSII supercomplexes or core complexes appear in a minority of the membranes (see [8] for a list of native crystalline arrays, [10]). A study of paired inside-out grana membranes indicated that crystalline arrays of adjacent layers can have a specific interaction in which orientations of opposing PSII complexes have preferred angles. This was found for spinach [11] as well as for *Arabidopsis* membranes [12]. A tomographic study on isolated spinach thylakoid membranes revealed the presence of the PSII crystalline arrays exclusively in stacked grana membranes, indicating the importance of a specific interaction between the stroma membrane surfaces of two adjacent membrane layers for the formation of regular PSII arrays [10]. In addition, recent experiments indicate that the PsbS protein controls the frequency of this crystalline macro-organization in the grana membrane [13]. High levels of PsbS disrupt the macro-organization. However, many other aspects of the PSII distribution,

*Abbreviations:* PSII, photosystem II; LHCII, light harvesting complex II; C, photosystem II core complex; S, strongly bound trimeric LHCII; M, moderately bound trimeric LHCII

* Corresponding authors. Tel.: +31 50 3634225; fax: +31 50 363 4800.
*E-mail addresses:* r.kouril@rug.nl (R. Kouřil), e.j.boekema@rug.nl (E.J. Boekema).

0005-2728/$ – see front matter © 2010 Elsevier B.V. All rights reserved.
doi:10.1016/j.bbabio.2010.11.007

such as possible changes upon state transition or photoinhibition are not known in detail. Recently, however, the mobility of grana membrane proteins was studied by fluorescence recovery after photobleaching [14]. In intact, wild-type chloroplasts a mobile population of grana membrane proteins increases significantly after photoinhibition, which is consistent with a role of protein diffusion in the PSII repair cycle. It was shown that protein phosphorylation switches the membrane system to a more fluid state, thus facilitating the PSII repair cycle [14].

There is a generally accepted idea that the entire thylakoid membrane is folded in such a way that it encloses a single aqueous space, the thylakoid lumen. The space between the thylakoid membrane and the chloroplast envelope is called the stroma. The details of the thylakoid membrane folding and the interconnection of grana stacks with stromal thylakoids have not been totally solved. Early electron microscopy studies of serial sections of chemically fixed thylakoid membranes led to the proposition of several 3D models of thylakoid membrane architecture (reviewed in [15]). Afterward, some of these models were questioned by an electron microscopy study of freeze-substituted chloroplast sections [16]. These models include (i) "the folded membrane model", which proposes a way of a dynamic reversible folding of the thylakoid membrane [17] and (ii) "the helical model", in which the stroma membranes are wound around the granal stacks [15]. It was further proposed that a bifurcation of stromal membranes and a subsequent membrane bending and fusion is involved in grana stack formation [16]. These novel viewpoints of the grana architecture initiated a further discussion with a common consensus that current data still require further refinements to clarify discrepancies between individual models [18–20]. Refining of chloroplast membrane topology models will depend very much on improving of electron microscopy hardware to reach better data acquisition and on perfecting tomography reconstruction techniques, necessary to image complete chloroplasts.

Over the last decade the application of cryo electron tomography on intact frozen-hydrated samples has become a popular technique to visualize cell structures because the method is free of fixation artifacts [21]. In combination with sub-volume averaging, it is nowadays a very feasible approach for studying macromolecules and membrane architecture inside cells, cellular organelles and structures of membrane protein complexes in their native membrane environment [10,22–25]. Because electron tomography is most efficient with thin objects and since there is a direct relation between the size of an object and the theoretical resolution [26], it works the best for small objects up to about 0.5–1 μm. Unfortunately, chloroplasts are substantially larger and also densely packed with membranes. Hence, intact chloroplasts are currently just too large to yield a resolution of about 50–60 Å, which is necessary to unambiguously elucidate structural features of the thylakoid membrane, including its precise folding. In this study, we applied cryo electron tomography to isolated grana membrane stacks. Working with smaller tomography volumes, in contrast to e.g. intact chloroplasts, allowed pushing up the resolution to see interpretable densities of PSII complexes in the granal membrane. This enabled averaging sub-volumes containing PSII and seeing characteristic features of PSII core complexes in the natural membrane at 40 resolution. In addition, single particle 3D averaging revealed a novel density associated with the PSII core complex in multiple copies, which has not been observed before in isolated forms of PSII complexes. Comparison of the 3D structure of the PSII core complex with the recently proposed pseudo-atomic model of the complete, $C_2S_2M_2$ PSII supercomplex [7] revealed a striking fit of the extra densities with the position of LHCII trimers. A possible origin of the novel density is discussed.

## 2. Materials and methods

### 2.1. Preparation of the granal thylakoid membranes

Thylakoid membranes were isolated from market, dark adapted spinach according to [27]. The isolated membranes were resuspended in 20 mM Bis-Tris (pH 6.5) with 5 mM $MgCl_2$ at a final concentration of 0.5 mg of Chl/mL and partially solubilized with digitonin at a final concentration of 0.5% (w/v) for 20 min at 4 °C with a slow stirring, followed by centrifugation in an Eppendorf table centrifuge for 15–20 min [28]. The pellet, which contained the non-solubilized granal thylakoid membranes, was used for cryo electron tomography.

### 2.2. Cryo electron tomography

Granal thylakoid membranes were mixed with 10-nm gold particles as fiducial markers and applied to glow discharged 200 mesh Quantifoil specimen support grids (Quantifoil Micro Tools GmbH) coated with a thin carbon film. Vitrification was performed in liquid ethane using a Vitrobot Mk3 (FEI company, Eindhoven) operating under a 100% humidified atmosphere at room temperature. Electron tomography was performed on a 300 kV G2 Polara electron microscope (FEI) equipped with a Gatan post-column energy filter. Images were recorded with a 2 k×2 k CCD camera (Gatan) at 8 μm underfocus and 51,750x final magnification, resulting in a pixel size of 0.58 nm at the level of the specimen. Single axis tilt series were recorded at 2° increments over a range of ±68° with a total dose of about 80 $e/Å^2$.

### 2.3. 3D reconstruction and image analysis

Tomograms were calculated using IMOD software [29] and further denoised with 20 iterations by non-linear anisotropic diffusion [30]. Averaging of manually selected sub-volumes with a box size of either 232×232 Å or 319×319 Å was performed using PEET program (a part of IMOD package). Central coordinates of the sub-volumes were selected using 3dmod program. Surface views of averaged sub-volumes were produced using 3dmod program (a part of the IMOD package). The resolution of the final averaged sub-volume was estimated by Fourier Shell Correlation [31] at 0.3 threshold with EMAN software [32].

## 3. Results

### 3.1. Cryo electron tomography of granal thylakoid membranes

Suspensions of isolated granal thylakoid membranes (Supplemental Fig. 1) were directly investigated by cryo electron tomography. Fig. 1 shows four slices of a typical electron tomogram of one granal membrane stack, where four membrane layers were clearly resolved (Fig. 1A to D). This and other tomographic reconstructions revealed distinct densities in all membrane layers, which could be unambiguously assigned to the dimeric PSII complex (see e.g. white arrows in Fig. 1A). Tomographic slices of the middle part of the reconstruction indicate that the membranes form two vesicles, as evident from a pair of strong rims resolved at the edge of the granal membrane (Figs. 1B and C). Close investigation of the tomographic data revealed other interesting features that will be discussed below.

Creation of surface views of individual granal stacks gave good insight into the overall 3D organization. Fig. 2 shows different angular surface views of two granal vesicles like in Fig. 1, with marked positions of individual PSII complexes (Figs. 2A to C, and D to F, respectively). Both vesicles have the shape of a sac and each one is formed by a pair of continuous membranes, which does not have any direct contact with the other. The outer membrane, depicted in green, accommodates PSII complexes in both the upper and bottom membrane layers (Fig. 2, green and blue spheres, respectively). The outer membrane is not (anymore) continuous at the vesicle margin, which is mainly obvious from the top-views (Figs. 2A and D). The inner membrane, depicted in brown, encloses the inner space of the vesicle and accommodates PSII complexes in two layers (Fig. 2, cyan and red spheres). At this moment, it is not clear (due to a resolution-limited membrane tracking) if the inner membrane fully encloses the

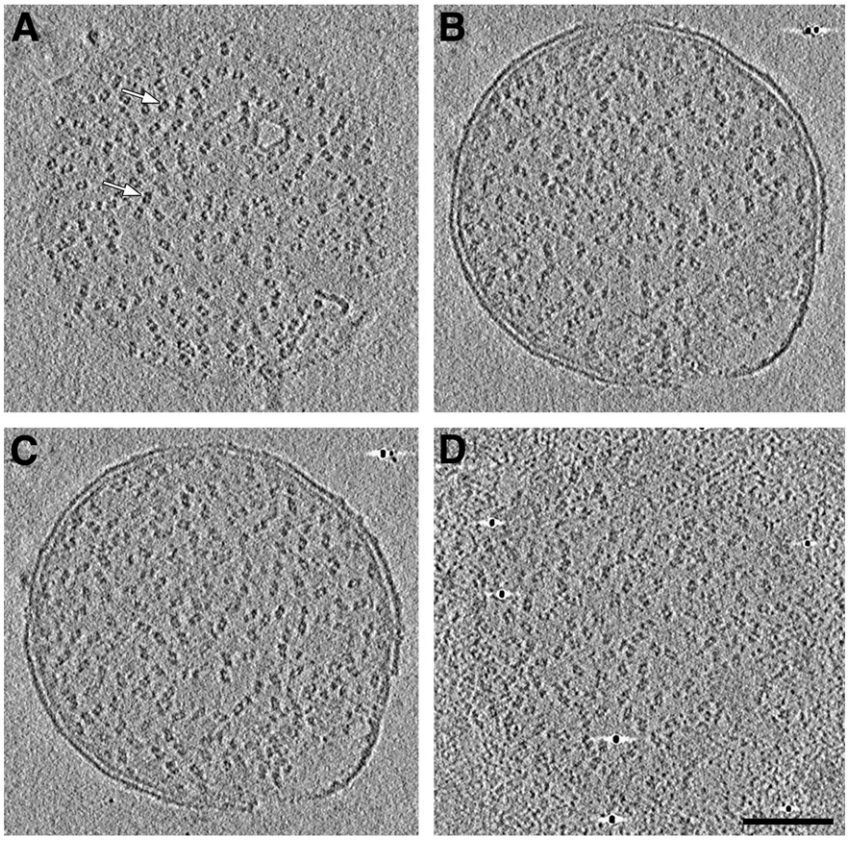


**Fig. 1.** Tomographic slices of a stack of four granal membranes forming two vesicles. An example of X–Y slices of 2.9 nm thickness along the z-axis projection from tomographic reconstruction of an ice-embedded spinach granal membrane vesicle, which contains four membrane layers: (A) the upper membrane of the granal vesicle. (B–C) adjacent membrane layers in the middle of the granal vesicle. (D) the bottom membrane of the granal vesicle facing a thin carbon support film. PSII complexes were well resolved in all four membrane layers (see e.g. white arrows in A). The bar is 100 nm.

inner space of the vesicle or if there is a narrow gap in the membrane, which would connect the inner space with surroundings. Under the experimental conditions applied, the distance between two outer adjacent PSII layers (one layer formed by the outer and the other formed by the inner membrane) was found in these (Figs. 2A–C and D–F) and similar reconstructions to be rather constant in a range of 14–16 nm. In contrast, the distance between adjacent PSII layers formed only by the inner membrane was highly variable in 8 different reconstructions, of which two extremes are shown (Figs. 2C and F). This is probably because the vesicles of thylakoid membranes can get swollen during isolation procedure (see also [10]). The integrity of grana membrane stacking may also have been alterated by the detergent solubilization of the connecting stroma membranes. Nevertheless, some characteristics remain, such as the remarkable flatness of each single membrane leaflet (Fig. 2).

### *3.2. 3D analysis of PSII complexes*

Tomogram sub-volumes of randomly orientated PSII were selected and subjected to 3D analysis and subsequent averaging. Fig. 3 shows the result of the analysis. Averaging of the best 100 sub-volumes revealed the structure of the dimeric PSII core complex (Figs. 3A to C). Views of the PSII complex from the lumenal (Fig. 3A), the stromal side (Fig. 3B) and from a side (Fig. 3C) clearly show the topology of the PSII core part, especially of the extrinsic subunits of the oxygen evolving complex protruding into the lumen. Noteworthy, the 3D analysis revealed a pair of additional spherical densities at the lumenal membrane surface close to the center of the PSII complex (Figs. 3A–C). Comparison of the 3D structure of the PSII complex with the recently proposed pseudo-atomic model of the complete, $C_2S_2M_2$ PSII super-complex [7] indicates an overall structural similarity of the 3D tomography data with the higher-resolution model of the super-complex (Fig. 3D). Furthermore, the comparison revealed a striking fit of the extra spherical densities with the position of the S-type of LHCII trimers centers. Analysis of the same 100 sub-volumes, but with a larger box size to cover a larger space around the PSII core, revealed another pair of non-membrane embedded densities, which coincided well with the position of the M-type LHCII trimers in the pseudo-atomic model (Fig. 3E). Extension of the box size was, however, at the expense of the resolution, which was computed to be 40 for the core part in case of analysis of smaller sub-volumes. Features of individual LHCII trimers within the membrane could not be revealed, possibly because of low contrast.

## 4. Discussion

Imaging of organelles in amorphous ice, free of any fixation agent, represents a situation close to the natural state. We have previously shown that it is feasible to average sub-volumes containing large macromolecules from intact organelles, such as dimeric ATP synthase in mitochondria from the alga *Polytomella* [24]. In present study, we investigated a fraction of isolated spinach granal membranes using cryo electron tomography to able to resolve and analyze PSII complexes in their native environment and native form. The reason to work here with fragments was a practical one, because the *Spinacea* chloroplasts turned out to be just too thick to image them as entities. It was already shown that to compensate for this limitation, working with small thylakoid membrane fractions is an appropriate way to yield enough resolution in tomographic reconstruction [10], compared to analysis of thin sections of chemically fixed (reviewed in [15]) or high-pressure frozen, freeze-substituted chloroplast sections [16].

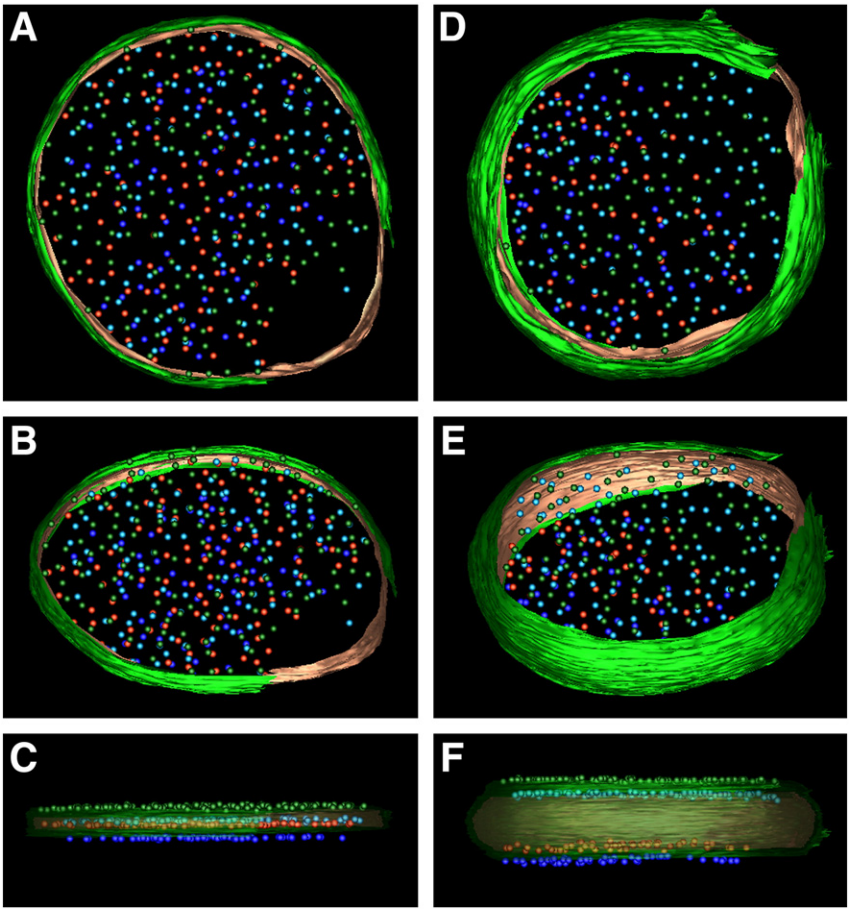


**Fig. 2.** Surface views of two reconstructed granal stacks (A–C and D–F), composed of two granal membrane vesicles of different thickness. Reconstructions are seen in top view (A, D), tilted view (B, E) and side-view (C, F) orientation, respectively. The outer and inner membranes are depicted in green and brown, respectively. PSII complexes were resolved in four membrane layers and are depicted as green, cyan, red, and blue spheres.

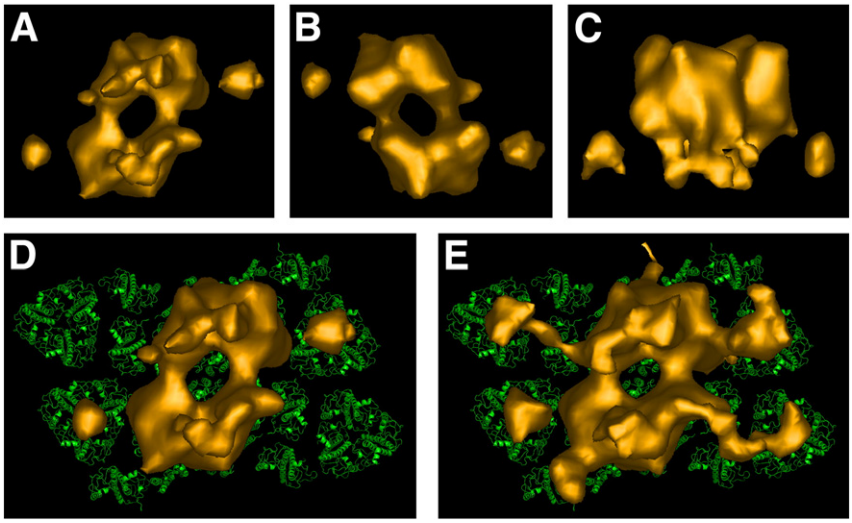


**Fig. 3.** 3D data of PSII complex and fitting. (A–C) 3D average of the best 100 sub-volumes of PSII complexes selected from tomographic reconstructions viewed from the lumenal and stromal side, and from a side along the membrane plane, respectively. Isosurface model shows the PSII core complex together with extrinsic subunits of oxygen-evolving complex resolved on the lumenal side of the complex. Further, two additional spherical densities were revealed at the lumenal side of the PSII complex. (D) a comparison of the isosurface model of PSII complex with a pseudo-atomic model of the complete PSII supercomplex ($C_2S_2M_2$ supercomplex) [7], viewed from the lumenal side. The fit indicates that the spherical densities coincide with the position of the S-type LHCII trimers. (E) a comparison of the isosurface model of PSII complex obtained from the average of PSII sub-volumes of an increased size (with respect to the model presented in A–D) with the pseudo-atomic model of the complete PSII supercomplex. Analysis of the larger sub-volumes revealed additional, non-membrane embedded spherical densities, which coincide with the position of the M-type LHCII trimers. Analysis of larger sub-volumes was at the expense of the resolution of the PSII core complex and extrinsic subunits of oxygen-evolving complex.

The potency of the cryo electron tomography approach applied on non-chemically fixed chloroplasts is also obvious from the current data. Imaging of single grana discs free of any fixation agent led to a resolution which is far better than previously obtained by thin section studies of chemically fixed chloroplasts. This is evident from the appearance of individual PSII core complexes in the membrane which could not be resolved before. This is mainly due to using smaller volumes [33], but also because of better instrumental performance. Especially, the application of energy filtering to remove inelastically scattered electrons that blur the image is beneficial for a higher resolution in electron tomography [34].

### 4.1. 3D analysis of PSII complexes revealed novel densities

The high-resolution structure of the PSII core complex of cyanobacteria was recently improved to 2.9 Å resolution [35]. In contrast, the structural analysis of plant PSII supercomplex is impaired mainly by its lability and the complexity of its peripheral antenna system (see Introduction). A novel protocol for obtaining homogeneous fractions of the various types of PSII-LHCII supercomplexes enabled a 2D structural characterization of the largest $C_2S_2M_2$ PSII supercomplex from *Arabidopsis* at 12 Å resolution [7]. Previously, 3D electron microscopy structural studies yielded a 17 Å resolution 3D map for the smaller $C_2S_2$ PSII supercomplex [6]. It is known, however, that PSII easily may lose some of its subunits upon purification [36]. Here, we show a 3D analysis of plant PSII complex, which was resolved in the native thylakoid membrane by cryo electron tomography. The averaging of 3D sub-volumes revealed the structure of PSII complex at 40 Å resolution (Fig. 3), which was assigned as the PSII core complex, based on the comparison with the recently proposed pseudo-atomic model of the complete, $C_2S_2M_2$ PSII supercomplex [7]. An overall architecture of lumen-exposed oxygen evolving complex indicates similar features as observed in a 3D map of plant PSII supercomplex [5,6].

The averaging of 3D sub-volumes revealed extra densities on both sides of the dimeric core. These densities must be genuine proteins, because (1) they are at positions related by two-fold rotational symmetry and (2) this symmetry was not imposed during averaging or afterwards. They are too large to be considered as lumen-exposed loops of LHCII. Comparison with the pseudo-atomic structure reveals that these proteins are associated to the PSII supercomplexes, right on top of the S- and M-trimers (Figs. 3D and E). We can be quite confident that most LHCII trimers have the extra lumenal density, because the 3D averaging is performed on all selected sub-volumes, including those who may have LHCII trimers without such densities. If for instance only 25% of the trimers would have a density, then the other 75% would cause that in the final sum this detail would have been more or less lost.

As the extra densities are attached to the lumenal side of the PSII supercomplex (Fig. 3C), they likely represent an enzyme. Although a proteome analysis indicates that the lumen compartment can contain up to 200 different proteins [37] we tentatively propose that the extra densities represent, due to their specific association to LHCII proteins, violaxanthin deepoxidase (VDE). VDE is a soluble lumenal protein, which is involved in the conversion of violaxanthin into zeaxanthin in the xanthophyll cycle and thus in non-photochemical quenching of an excess of excitation energy (see [38] for recent review). It was found that VDE remains attached to the thylakoid membrane at acidic pH, even after several freeze-thaw cycles [39]. Under our experimental conditions, all tomography experiments were performed at pH = 6.5, which was shown to still keep VDE in the bound form [39]. On the other hand, it remains puzzling that each LHCII trimer would have a VDE copy, as enzymes are usually present in much smaller numbers than proteins, such as the LHCII trimers. It will take more effort to assign the nature of the extra densities and the most obvious way to solve the problem is by using *Arabidopsis* null mutants.

### 4.2. Nature and distribution of the PSII complexes in the thylakoid membrane

Grana discs were obtained after a short treatment with a mild detergent to get them separated. Tomographic reconstructions revealed that grana discs consist of two concentrically folded membranes, which form a sac with four layers (Figs. 1 and 2). Densities of PSII core complexes were clearly resolved in all four membrane layers. The tomographic data not only revealed the positions of individual PSII complexes within the native membrane, but showed clearly recognizable details of individual molecules. Importantly, the features of dimeric PSII core complexes provide the orientations of the PSII dimers within the membrane plane (Fig. 4). This led us to correlate the map of the large $C_2S_2M_2$ PSII supercomplex with the PSII cores. Hand fitting of this specific supercomplex contour indicates that there would be enough space to accommodate complete PSII supercomplexes on many of the cores (Fig. 4A, green contours). In several cases, however, $C_2S_2M_2$ particles overlap with their neighbors (Fig. 4A, red contours). In most of them, only smaller PSII supercomplexes can be present (e.g. $C_2S_2$ or $C_2S_2M$ supercomplexes), because of overlapping antennae. The number of smaller

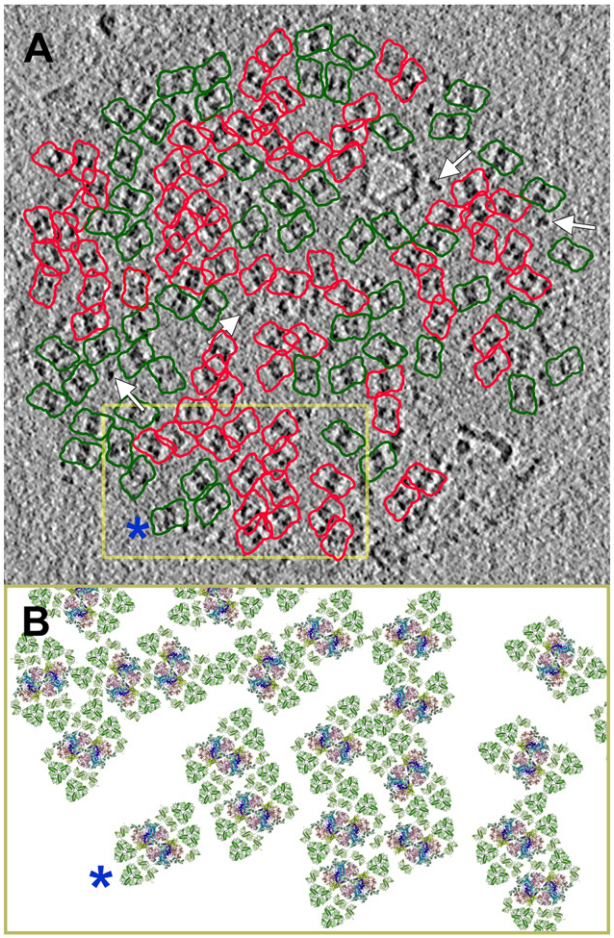


**Fig. 4.** Distribution of PSII complexes in thylakoid membrane. (A) superimposition of contours of the complete, $C_2S_2M_2$ supercomplex over clearly resolved densities of the PSII core in one membrane layer of the thylakoid stack of Fig. 1. Green and red contours indicate positions of PSII complexes with either no or significant clashes with neighboring PSII complexes, respectively. White arrows indicate smaller, non-assigned densities, which could represent e.g. PSII monomers. (B) example of the higher organization of PSII supercomplexes in the thylakoid membrane based on the experimental data. Blue asterisk indicates the corresponding PSII complex within the selected area of the tomographic data (see yellow box in A).

complexes is estimated to be about half of red marked particles, or 23% of the total. Furthermore, tomographic data revealed also smaller densities, which cannot be assigned to PSII dimers, and likely represent monomeric PSII complexes (Fig. 4A, white arrows). The fact that not all of the PSII core complexes can be surrounded by a complete set of four LHCII trimers is in line with previous work on solubilized spinach chloroplast membranes [40]. However, in that particular study only 1% of the particles was assigned as $C_2S_2M_2$ supercomplexes and the vast majority of PSII particles (70%) was comprised of the smaller $C_2S_2$ complexes. It is well possible that the absolute amount of supercomplexes became decreased by detergent solubilization; thus our tomographic data provide a closer-to-reality view of the grana membrane (Fig. 4A). However, it should also be realized that light conditions have a strong influence on the amount of free- and bound LHCII [41], which can cause different amounts of individual types of PSII supercomplexes.

It is also evident that regardless of a minor fraction of unassigned densities, PSII supercomplexes do not occupy the whole surface of grana membrane (Fig. 4B). There are several membrane areas, which are very flat and seem to be free of protruding proteins. They can represent membrane lipid areas, which are important for a lateral diffusion of proteins and plastoquinone molecules in the membrane, or they can be partially occupied by free LHCII proteins, as pointed out earlier [3]. Thus, there appears to be ample space for the non-bound fraction of LHCII trimers, as was already suggested two decades ago [42].

Within the reconstructed volumes there were no highly ordered crystalline domains of individual PSII complexes present, except of one tomogram, where some clear rows of PSII molecules were seen (Supplemental Fig. 2). The rows of PSII are similar to those observed before in isolated paired inside-out membranes [11,12]. It is highly unlikely that a mild detergent treatment in the purification procedure has a negative effect on the crystallinity, as the ordered PSII arrays have been observed before in detergent treated samples, including the recent tomography data [10]. However, such crystalline domains usually occupy only a small part of all grana membranes [10,11,13] and their presence is mostly a matter of lateral segregation within the densely packed membranes [3]. Although in these particular membranes the distribution and orientation of PSII complexes is seemingly random, the fitting indicates there is some preference for a parallel alignment (Fig. 4), which is in line with statistical analysis of AFM data [9].

### 4.3. Architecture of the granal stacks by cryo electron tomography

The total folding of the grana membrane remains certainly an intriguing question to address by any microscopy technique. In our study, we could not address the question of the complete architecture of the granal thylakoids by using cryo electron tomography because the *Spinacea* chloroplasts turned out to be just too thick to image them as entities. Therefore, we compromised with working on thin grana stacks from disrupted chloroplasts. The use of detergent in our experiments led to removal of stroma thylakoids, which made it impossible to reconstruct how the grana membranes interconnect the unstacked stroma membranes. Disruption probably also lead to an alteration of membrane stacking and thus to variation in the distances between the different membranes (Figs. 2 and 5), as is evident from other studies [43].

Nevertheless, tomographic reconstructions on the thinner moiety of grana stacks revealed that many grana discs consist of two concentrically folded membranes, which form a sac with four layers (Figs. 1, 2 and 5), although some thicker ones were also observed. Densities of PSII core complexes were clearly resolved in all four membrane layers with no obvious sign for a higher ordered organization (Fig. 1 and 4, see below for a discussion). Crucial for a thorough examination of the overall thylakoid structure is the fact that the stroma and lumen sides of the membrane could be established from the PSII orientation, which was derived from 3D analysis of PSII sub-volumes selected from individual membrane layers. 3D analysis clearly indicated that the two folded membranes are facing each other from their lumen sides as illustrated in our schematic models (Fig. 5A,B). The thickness of the lumen space was found rather constant, in a range of 14–16 nm, which is in a range reported for thylakoid membranes isolated from dark adapted plants [3]. In contrast, the dimension of the stroma space was found rather variable (Figs. 2C and F; 5A). Considering the dimensions of the oxygen evolving complex (about 5 nm in a direction perpendicular to the membrane plane), there is no spatial restriction for the distribution of PSII complexes in the adjacent layers. Thus, under applied experimental conditions, a juxtaposition of PSII complexes is also possible. A smaller distance is not expected simply due to the presence of the novel densities on top of the LHCII trimers. Only in the absence of such densities, the PSII supercomplexes would have the possibility to approach closer, as claimed in [10].

Tomographic data further indicate that in the margins of the grana discs the pair of membranes is separated by only 3–4 nm (Figs. 1 and 5) and free of PSII complexes, a firm proof for the hypothesis that the margins are free from the major proteins involved in the light reactions in photosynthesis [3].

The appearance of crystalline arrays, discussed in Section 4.2., is often within two adjacent layers [11,12]. In previous studies, it was found that PSII complexes from two such layers with semi-crystalline arrays also show preferential orientations in their interaction in the stroma [11,12]. This was also confirmed by recent tomography study [10], where it was discussed that electrostatic interactions of LHCII trimers are responsible for this. The 3D data of Fig. 3A allow us to see trends in the lateral distribution of PSII protein complexes of four intact layers. The interaction of PSII complexes of the layers separated by the narrow stromal space (Fig. 2C) could, in principle, also be specific. The current data, however, do not show any obvious relation

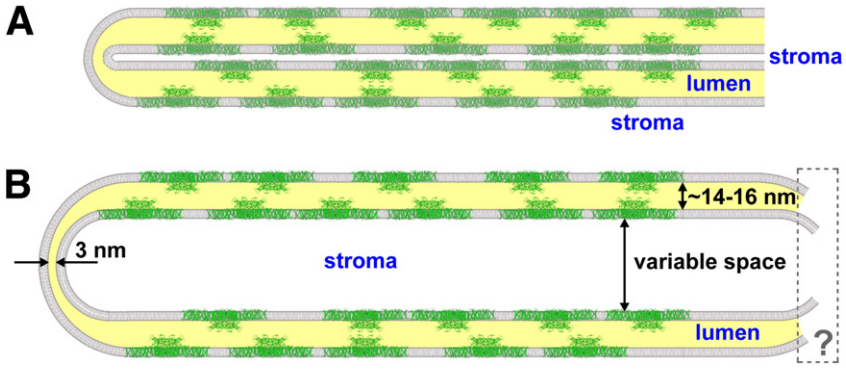


**Fig. 5.** Scheme of the stacking of membranes in two reconstructed granal stacks of different thickness. The same stacks are presented in Fig. 2. The stroma and lumen sides of the membranes were established from the orientations of the PSII complexes in sub-volumes as indicated in the picture; the $C_2S_2M_2$ supercomplexes are depicted on scale. (A) schematic representation of the granal stack from Fig. 2A. (B) schematic representation of the granal stack from Fig. 2B. The box at the right indicates that the membranes were locally not continuous.

in orientation of PSII complexes from adjacent layers. Apparently, the interaction of single PSII complexes, randomly distributed in grana membranes is different from stacked semi-crystalline arrays.

### 4.4. Conclusions and outlook

Combination of cryo electron tomography on intact ice embedded samples with 3D analysis of sub-volumes clearly represents a powerful approach for structural studies close to native conditions. It can reveal novel structures of transient and unstable assemblies, which have not been observed before in studies of isolated protein complexes obtained even under optimized conditions. Our tomography data provide the most detailed information on PSII within grana membranes until now. But further investigation of more intact grana stacks is necessary to disclose the nature and formation of their architecture, which will extend our current and simplified views [3,18–20]. In the future, it should be technically feasible to record tomography data on complete chloroplasts at a resolution as provided here, which was performed with current best technology. It should be performed on already existing microscopes equipped with a higher acceleration voltage than the 300 kV applied here to be able to penetrate thicker samples. A more crucial factor necessary to get the good resolution is the use of a direct electron counting camera [44], instead of current CCD camera technology, expected to become available in 2011 and to have a 10x better performance. Thus it may be possible to provide an improved view on grana stacks with interconnected stroma membranes which may lead to refined models of how green plant photosynthesis is carried out at the membrane level.

Supplementary materials related to this article can be found online at doi:10.1016/j.bbabio.2010.11.007.

## Acknowledgments

Work was supported by a grant of the Netherlands Organization of Scientific Research NWO. We thank Dr. Jan Dekker and Dr. Alexander Ruban of the HARVEST network for discussions.

## References

[1] P.Å. Albertsson, A quantitative model of the domain structure of the photosynthetic membrane, Trends Plant Sci. 6 (2001) 349–354.
[2] S. Jansson, The light-harvesting chlorophyll a/b binding proteins, Biochim. Biophys. Acta 1184 (1994) 1–19.
[3] J.P. Dekker, E.J. Boekema, Supermolecular organization of the thylakoid membrane proteins in green plants, Biochim. Biophys. Acta 1706 (2005) 12–39.
[4] E.J. Boekema, H. van Roon, F. Calkoen, R. Bassi, J.P. Dekker, Multiple types of association of photosystem II and its Light-Harvesting antenna in partially solubilized Photosystem II membranes, Biochemistry 38 (1999) 2233–2239.
[5] J. Nield, E.V. Orlova, E.P. Morris, B. Gowen, M. van Heel, J. Barber, 3D map of the plant photosystem II supercomplex obtained by cryoelectron microscopy and single particle analysis, Nat. Struct. Biol. 7 (2000) 44–47.
[6] J. Nield, M. Balsera, J. De Las Rivas, J. Barber, Three-dimensional electron cryomicroscopy study of the extrinsic domains of the oxygen-evolving complex of spinach, J. Biol. Chem. 277 (2002) 15006–15012.
[7] S. Caffarri, R. Kouřil, S. Kereïche, E.J. Boekema, R. Croce, Functional architecture of higher plant photosystem II supercomplexes, EMBO J. 28 (2009) 3052–3063.
[8] L. Bumba, F. Vácha, Electron microscopy studies of Photosystem II, Photosynth. Res. 77 (2003) 1–19.
[9] H. Kirchhoff, S. Lenhert, C. Büchel, L. Chi, J. Nield, Probing the organization of photosystem II in photosynthetic membranes by atomic force microscopy, Biochemistry 47 (2008) 431–440.
[10] B. Daum, D. Nicastro, J. Austin, J. McIntosh, W. Kühlbrandt, Arrangement of Photosystem II and ATP Synthase in chloroplast membranes of Spinach and Pea, Plant Cell 22 (2010) 1299–1312.
[11] E.J. Boekema, J.F.L. van Breemen, H. van Roon, J.P. Dekker, Arrangement of PSII supercomplexes in crystalline macrodomains within the thylakoid membrane of green plants, J. Mol. Biol. 301 (2000) 1123–1133.
[12] A.E. Yakushevska, P.E. Jensen, W. Keegstra, H. van Roon, H.V. Scheller, E.J. Boekema, J.P. Dekker, Supermolecular organization of photosystem II and its associated light-harvesting antenna in *Arabidopsis thaliana*, Eur. J. Biochem. 268 (2001) 6020–6021.
[13] S. Kereïche, A.Z. Kiss, R. Kouřil, E.J. Boekema, P. Horton, The PsbS protein controls the macro-organisation of photosystem II complexes in the grana membranes of higher plant chloroplasts, FEBS Lett. 584 (2010) 759–764.
[14] T.K. Goral, M.P. Johnson, A.P.R. Brain, H. Kirchhoff, A.V. Ruban, C.W. Mullineaux, Visualizing the mobility and distribution of chlorophyll proteins in higher plant thylakoid membranes: effects of photoinhibition and protein phosphorylation, Plant J. 62 (2010) 948–959.
[15] L. Mustardy, G. Garab, Granum revised. A three-dimensional model — where things fall into place, Trends Plant Sci. 8 (2003) 117–122.
[16] E. Shimoni, O. Rav-Hon, I. Ohad, V. Brumfeld, Z. Reich, Three-dimensional organization of higher-plant chloroplast thylakoid membranes revealed by electron tomography, Plant Cell 17 (2005) 2580–2586.
[17] P.O. Arvidsson, C. Sundby, A model for the topology of the chloroplast thylakoid membrane, Aust. J. Plant Physiol. 26 (1999) 687–694.
[18] L. Mustardy, K. Buttle, G. Steinbach, G. Garab, The three-dimensional network of the thylakoid membranes in plants; quasihelical model of the granum-stroma assembly, Plant Cell 20 (2008) 2552–2557.
[19] V. Brumfeld, D. Charuvi, R. Nevo, S. Chuartzman, O. Tsabaki, I. Ohad, E. Shimoni, Z. Reich, A note on three-dimensional models of higher-plant thylakoid networks, Plant Cell 20 (2008) 2546–2549.
[20] G. Garab, C.A. Mannella, Reply: On three-dimensional models of higher-plant thylakoid networks: Elements of consensus, controversies, and future experiments, Plant Cell 20 (2008) 2549–2551.
[21] O. Medalia, I. Weber, A.S. Frangakis, D. Nicastro, G. Gerisch, W. Baumeister, Macromolecular architecture in eukaryotic cells visualized by cryoelectron tomography, Science 298 (2002) 1209–1213.
[22] M. Beck, F. Förster, M. Ecke, J. Plitzko, F. Melchior, G. Gerisch, W. Baumeister, O. Medalia, Nuclear pore complex structure and dynamics revealed by cryoelectron tomography, Science 306 (2004) 1387–1390.
[23] M. Strauss, G. Hofhaus, R.R. Schröder, W. Kühlbrandt, Dimer ribbons of ATP synthase shape the inner mitochondrial membrane, EMBO J. 27 (2009) 1154–1160.
[24] N.V. Dudkina, G.T. Oostergetel, H.P. Braun, E.J. Boekema, Row-like organization of ATP synthase in intact mitochondria determined by cryo-electron tomography, Biochim. Biophys. Acta 1797 (2010) 272–277.
[25] N.V. Dudkina, R. Kouřil, J.B. Bultema, E.J. Boekema, Imaging of organelles by electron microscopy reveals protein–protein interactions in mitochondria and chloroplasts, FEBS Lett. 584 (2010) 2510–2515.
[26] A. Klug, R.A. Crowther, 3-dimensional image reconstruction from viewpoint of information theory, Nature 238 (1972) 435–440.
[27] H. van Roon, J.F.L. van Breemen, F.L. de Weerd, J.P. Dekker, E.J. Boekema, Solubilization of green plant thylakoid membranes with n-dodecyl-D-maltoside. Implications for the structural organization of the Photosystem II, Photosystem I, ATP synthase and cytochrome *b6 f* complexes, Photosynth. Res. 64 (2000) 155–166.
[28] R. Kouřil, A. Zygadlo, A.A. Arteni, C.D. de Wit, J.P. Dekker, P.E. Jensen, H.V. Scheller, E.J. Boekema, Structural characterization of a complex of photosystem I and light-harvesting complex II of *Arabidopsis thaliana*, Biochemistry 44 (2005) 10935–10940.
[29] J.R. Kremer, D.N. Mastronarde, J.R. McIntosh, Computer visualization of three-dimensional image data using IMOD, J. Struct. Biol. 116 (1996) 71–76.
[30] A.S. Frangakis, R. Hegerl, Noise reduction in electron tomographic reconstructions using nonlinear anisotropic diffusion, J. Struct. Biol. 135 (2001) 239–250.
[31] M. van Heel, G. Harauz, Resolution criteria for 3-dimensional reconstruction, Optik 73 (1986) 119–122.
[32] S.J. Ludtke, P.R. Baldwin, W. Chiu, EMAN: Semiautomated software for high-resolution single-particle reconstructions, J. Struct. Biol. 128 (1999) 82–97.
[33] A. Leis, B. Rockel, L. Andrees, W. Baumeister, Visualizing cells at the nanoscale, Trends Biochem. Sci. 34 (2009) 60–70.
[34] R. Grimm, D. Typke, W. Baumeister, Improving image quality by zero-loss energy filtering: quantitative assessment by means of image cross-correlation, J. Microsc. 190 (1998) 339–349.
[35] A. Guskov, J. Kern, A. Gabdulkhakov, M. Broser, A. Zouni, A.W. Saenger, Cyanobacterial photosystem II at 2.9-Å resolution and the role of quinones, lipids, channels and chloride, Nat. Struct. Mol. Biol. 16 (2009) 334–342.
[36] E.J. Boekema, J. Nield, B. Hankamer, J. Barber, Localization of the 23 kDa subunit of the oxygen evolving complex of Photosystem II by electron microscopy, Eur. J. Biochem. 252 (1998) 268–276.
[37] J.B. Peltier, O. Emanuelsson, D.E. Kalume, J. Ytterberg, G. Friso, A. Rudella, D.A. Liberles, L. Söderberg, P. Roepstorff, G. von Heijne, K.J. van Wijk, Central functions of the lumenal and peripheral thylakoid proteome of Arabidopsis determined by experimentation and genome-wide prediction, Plant Cell 14 (2002) 211–236.
[38] P. Jahns, D. Latowski, K. Strzalka, Mechanism and regulation of the violaxanthin cycle: The role of antenna proteins and membrane lipids, Biochim. Biophys. Acta 1787 (2009) 3–14.
[39] A. Hager, K. Holocher, Localization of the xanthophyll-cycle enzyme violaxanthin de-epoxidase within the thylakoid lumen and bolition of its mobility by a (light-dependent) pH decrease, Planta 192 (1994) 581–589.
[40] E.J. Boekema, H. van Roon, J.F.L. van Breemen, J.P. Dekker, Supramolecular organization of photosystem II and its light-harvesting antenna in partially solubilized photosystem II membranes, Eur. J. Biochem. 266 (1999) 444–452.
[41] J.M. Anderson, Photoregulation of the composition, function, and structure of thylakoid membranes, Ann. Rev. Plant Physiol. 37 (1986) 93–136.
[42] G.F. Peter, J.P. Thornber, Biochemical evidence that the higher plant photosystem core is organized as a dimer, Plant Cell Physiol. 32 (1991) 1237–1250.
[43] R. Danielsson, P.Å. Albertsson, Fragmentation and separation analysis of the photosynthetic membrane from spinach, Biochim. Biophys. Acta 1787 (2009) 25–36.
[44] A.C. Milazzo, G. Moldovan, J. Lanman, L. Jin, J.C. Bouwer, S. Klienfelder, S.T. Peltier, M.H. Ellisman, A.I. Kirkland, N.-H. Xuong, Characterization of a direct detection device imaging camera for transmission electron microscopy, Ultramicroscopy 110 (2010) 741–744.